Available online at www.sciencedirect.com
ScienceDirect
Cement and Concrete Research 37 (2007) 63–70
Cement and Concrete Research

Microstructural characterization of leaching effects in cement pastes due to neutralisation of their alkaline nature Part I: Portland cement pastes

A. Hidalgo [a,*], S. Petit [b], C. Domingo [c], C. Alonso [a], C. Andrade [a]

[a] Instituto de Ciencias de la Construcción "Eduardo Torroja" CSIC. Serrano Galvache, 4, E-28033 Madrid, Spain
[b] Université de Poitiers, CNRS UMR 6532 HydrASA, 40, avenue du Recteur Pineau, F-86022 Poitiers Cedex, France
[c] Instituto de Ciencia de Materiales de Barcelona, CSIC, Campus UAB, 08193 Bellaterra, Spain

Received 28 March 2005; accepted 1 October 2006

Abstract

When concrete is exposed to the elements, its underlying microstructure can be attacked by a variety of aggressive agents; for example, rainwater and groundwater. The knowledge of concrete resistance to long term water aggression is necessary for predictions of their performance in different environments. This study aims to analyse the effects of leaching on the microstructure of Portland cement binders. Leaching of cement pastes was performed by an accelerated extraction leaching test that produces significant degradation and helps to achieve equilibrium or near-equilibrium conditions between the leachant medium and cement paste. FTIR spectroscopy, TG-DTA thermal analysis, low temperature nitrogen gas sorption, and geochemical modelling were used to characterize the microstructural changes produced in cement pastes at different equilibrium pHs reached during the leaching process.

Keywords: Durability; Portland cement; Microstructure; Hydration products; Leaching

1. Introduction

Calcium silicate hydrate (C–S–H) gel, together with portlandite ($Ca(OH)_2$) and alkalis, dominate the chemical properties of the aqueous phase in Portland cement pastes, and account for its high pH and calcium solubility. The pH of their pore solution is initially greater than 13 as a result of the dissolution of sodium and potassium hydroxides from the cement producing a highly alkaline condition in the groundwater in contact with these materials. This hyperalkaline stage is a short-term stage and, later, when these hydroxides have been removed, the pH would be expected to decrease to around 12.5 and would be controlled by the dissolution of other constituent minerals such as portlandite and C–S–H phases.

C–S–H gels are the main constituents of the hydrated Portland cement systems, characterized by a poor crystalline structure with a variable composition [1,2]. The CaO/SiO_2 (Ca/Si) ratio and the concentration of calcium ($[Ca^{2+}]$) control the type of C–S–H gel [3]. The stoichiometry of most of the C–S–H gels has been identified in the range of $0.66 < Ca/Si < 2$ [3–9]. Various structures of C–S–H gel have been proposed, but Taylor [1] gave the most accepted one, i.e., C–S–H (I) and C–S–H (II), which are similar to tobermorite and jennite, respectively. According to Taylor [1], for $Ca/Si = 0.66$, the structure of the C–S–H gel presents some analogy with tobermorite, a Te–Oc–Te structure (Te: tetrahedral; Oc: octahedral), with silicate tetrahedral sheets of SiO_2 linear chains associated to an octahedral sheet of CaO [10,11], but with some defects [12–15]. The chain length is supposed infinite. The silicate chains are constituted of dimers ($Si(Q^2)$) connected by bridging tetrahedron ($Si(Q^{2p})$) [1]. Silicate tetrahedrons ($Si(Q^{2p})$) are balanced by H^+. As in the smectite structure, aluminium may substitute silicon in the tetrahedral chains [11,12]. When the Ca/Si ratio increases from 0.66 up to 1, H^+ is substituted by calcium in the interlayer space. The shortening of the silicate chains arises from higher calcium content [16,17]. From $Ca/Si = 1.65$ and about $[Ca^{2+}] = 22$ mM/l, $Ca(OH)_2$ precipitates in equilibrium with the C–S–H gel. For

* Corresponding author. Tel.: +34 913020440; fax: +34 913020700.
E-mail address: ahidalgo@ietcc.csic.es (A. Hidalgo).

0008-8846/$ - see front matter © 2006 Elsevier Ltd. All rights reserved.
doi:10.1016/j.cemconres.2006.10.002

this ratio, the structure of the C–S–H is depicted only by silicate dimers because of the silica bridging tetrahedra ($Si(Q^{2p})$) are unstable [18].

According to literature [1], the mineral hydrates, which may be reasonably expected to form on complete hydration of ordinary Portland cement at 25 °C, are C–S–H gel with Ca/Si = 1.8 (jennite type), portlandite, AF_t ($3CaO{\cdot}Al_2O_3{\cdot}3CaSO_4{\cdot}32H_2O$), AF_m ($3CaO{\cdot}Al_2O_3{\cdot}CaSO_4{\cdot}12H_2O$), C_3AH_6 ($Ca_3Al_2O_{12}H_{12}$), and M_4AH_{10} ($Mg_4Al_2O_{17}H_{20}$), being aluminium the major element after calcium and silicon, in most cement compositions. Decalcification of cement paste is closely associated with leaching; some authors have indicated that, for cement based materials, decalcification of C–S–H gels proceeds until a constant value of Ca/Si ratio in the solid is reached [19,20]. As in clays, aluminium in C–S–H could substitute into either the octahedral calcium sites of the cationic CaO plane or the tetrahedral silicon sites. The possible generation of Ca–Al–Si rich colloid particles from leached cement hydrates has been recently observed by transmission electron microscopy [21]. The purpose of this paper is to study the structural evolution of amorphous solid phases during the leaching process using FTIR and TG/ATD analysis. Moreover, it is widely accepted that almost all the surface area of cement pastes comes from the highly porous phase C–S–H and that the pore structure of cementitious materials is strongly influenced by leaching. This aspect was also deeply studied in this work by N_2 adsorption/desorption measurements since it leads to structural information on the formed amorphous C–S–H phases.

2. Experimental

2.1. Materials

Spanish cement (CEM I-SR according to the European Standard ENV 197-1) and two types of mineral additions (fly ash, FA and silica fume, SF) were used for the testing program. Cement pastes were fabricated with a water/cement ratio of 0.35 and they were hydrated during 7 days in sealed conditions (98% relative humidity and 20±2 °C). Fly ash and silica fume were added to the paste mixtures on a cement replacement basis. Formulations of cement mixtures were: 100% CEM I-SR, 59% CEM I-SR + 41% FA, and 73% CEM I-SR + 7% FA + 20% SF. Chemical composition of mineral additions and cements used in this work is showed in Table 1.

X-ray diffraction analysis of the fly ash (not shown) indicated that it was mainly composed of mullite, quartz, magnetite, CaO, calcite and glassy phases.

Table 1
Chemical composition of cements and mineral additions

Chemical analysis (%)	SiO_2	Al_2O_3	Fe_2O_3	CaO (total)	MgO	SO_3	Na_2O	K_2O	CaO (free)
CEM I-SR	19.60	4.43	4.27	64.53	0.95	3.29	0.11	0.28	1.92
Fly ash	48.71	25.18	5.18	12.09	1.61	0.43	0.61	3.28	0.15
Silica fume	96.32	0.00	0.00	0.67	0.49	0.00	0.15	0.39	0.04

2.2. Methods

2.2.1. Leaching test

The accelerated leaching procedure consisted of a batch test performed in a closed system [22,23]. Hydrated cement mixes were ground and sieved until a particle size less than 32 μm was obtained; then 10 g of this solid (S) are mixed with deionised water (L) in a ratio S/L = 1, producing an homogeneous slurry. Accelerated tests were performed in these slurries by adding an acid (HNO_3 1N), at a rate of 0.5 ml min^{-1} with an automated titrator (Net Titrino 721 from Metrohm), and stirring the sample vigorously to favour continuous mixture of leachant and sample. In the case of nitric attack, an N_2 flow was maintained during the process to avoid carbonation. The evolution of pH was continuously recorded and liquid and solid phases were taken at different pHs (10 and 7) corresponding to progressive degradation stages. Samples were vacuum filtered through a 0.45 μm filter. The process of hydration of solid phases was interrupted in each case by "freezing" the sample with acetone and ethanol. Further analysis of the leachates and solid phases were carried out according to the requirements for each special case.

2.2.2. Chemical analysis of leachates

Na, K, Fe, Mg and Al were analysed by Atomic Absorption Spectrometry using an 1100B Perkin Elmer Spectrometer. Ca^{2+} and Si(aq) were analysed by a photometric method using EGTA and ammonium molibdate as complexants respectively. SO_4^{2-} was analysed by turbidimetry and total alkalinity was determined by titration with hydrochloric acid.

2.2.3. Geochemical modelling

Leachate chemical compositions were introduced in PHR QPITZ code [24], using the database HATCHES [25], in order to calculate the thermodynamic status of such solutions; that is, the saturation indexes of mineral phases. The reaction of the major elements during leaching was modelled in order to help the understanding of the chemical processes. Changes in the chemistry of major elements interact with changes in the chemistry of minor and trace elements.

2.2.4. Microstructural characterization

Mid Infrared spectra of reference and degraded cement mixes were obtained using a Nicolet Magna 510 Fourier transform IR spectrometer (FTIR) equipped with a DTGS detector and a CsI beamsplitter. For each sample, 256 scans were recorded in the 4000–250 cm^{-1} spectral range with a resolution of 4 cm^{-1}. The spectra of all the samples were measured using the 12 mm diameter undried KBr pellets (0.1 mg of sample and 150 mg of KBr).

Thermal analyses of materials were performed using a Thermal Analyzer STA 409 equipment from Netzsch. Thermogravimetric curves were determined using 50 mg samples at a heating rate of 4 °C/min, in dry CO_2 free of N_2 flowing at 100 ml/min.

The specific surface area and pore volume of both the starting samples and leached materials were determined by N_2

adsorption at 77 K (BET ASAP 2000 Micromeritics INC). Previous to measurements, all samples were dried under reduced pressure (<1 mPa) at 393 K for 5 h. Total specific surface area (S_T) was determined by the BET-method. Mesopore plus macropore volume (V_P) and mean pore diameter in a volume basis (D_m) were estimated by the BJH-method [26].

3. Results and discussion

3.1. Geochemical modelling

A change in paste mineralogy, due to a leaching process, may lead to a change in pore solution composition as a result of equilibrium shift. The use of thermodynamic models to make predictions of the pore solution chemistry of cement can considerably simplify the estimation of solution speciation, and, consequently, the calculation of chemical equilibrium states.

Chemical composition of leachates and saturation indexes of some mineral phases are presented in Tables 2 and 3 respectively. It was considered that the potentially precipitating minerals were those with the highest saturation index. The saturation level with respect to tobermorite when samples were leached until an equilibrium pH of 10 indicated that this solid phase was the precipitating phase at this degradation level. At this degradation level system was undersaturated in portlandite.

According to modelling, if leaching continues until an equilibrium pH of 7 is reached, C–A–S–H gels or zeolites (chabazite and CaP) are the potentially precipitating solid phases. At this degradation level, solution is undersaturated in ettringite and C–S–H gels.

3.2. FTIR

The structure of C–S–H gel is very complex with a variable Ca/Si ratio corresponding to different molecular structures. FT-IR spectroscopy is one of the most powerful techniques normally used for molecular characterization. Recently, FT-IR has been found to be very useful in delineating the complex chemistry involved in the cement due to the poor crystallinity of silicate hydrates [27].

In hydrated Portland cements, the main mid-IR bands for C–S–H gels appear at ~970 cm^{-1} (Si–O stretching vibrations of Q^2 tetrahedra), 660–670 cm^{-1} (Si–O–Si bending vibration, which is influenced by Si–O–Si angle and occupancy of neighboring sites), and 450–500 cm^{-1} [27]. These mid-IR bands change systematically in frequency and/or intensity with Ca/Si ratio in C–S–H, which is also related with silicate polymerization. Fig. 1 shows the mid-IR spectra for the mixture 100% CEM I-SR in the lower frequencies; in this case, the observed features provide useful information about Ca/Si ratio in C–S–H, silicate polymerization, and the presence of TO_4 tetrahedra in gel chains (T = Si or Al).

The band at 970 cm^{-1} is attributed to Si–O stretching vibrations in C–S–H gels with jennite type structure. Amorphous aluminosilicate phases are likely to cause vibration at around 1070–1080 cm^{-1} since similar band position can be observed for natural and glassy aluminosilicate materials [28]. It is also suggested that the appearance of a shoulder at ~1200 cm^{-1} occurs for gels C–A–S–H with structure 1.1 nm tobermorite type (Ca/Si<0.8), because of its occurrence for natural aluminosilicates [29]. Thus, the shift of 970 cm^{-1} band, in reference sample, to ~1070 cm^{-1} in leached sample at pH 7 and the appearance of a shoulder at ~1200 cm^{-1}, can be attributed to C–S–H chain polymerization (which is accompanied of a decrease in Ca/Si ratio) and replacement of Al by Si producing an Al–tobermorite type structure.

Kalousek [30] first demonstrated that Al enters the structure of tobermorite. Diamond et al. [31] reported that Al can replace 15% of the Si contained in the tobermorite structure in samples hydrothermally treated and that this replacement increases the basal spacing. Hydrogarnet was found to appear as an additional phase when more than 10% of Si was replaced by Al [30]. The increase of basal spacing could also be produced because of the highly localized negative charge on the Si–O surfaces resulting from Si substitution by Al, and the repulsion between parallel surfaces.

Table 3
Saturation indexes of some cementitious hydrates

Mineral	Formula	pH	100% CEM I-SR	59% CEM I-SR 41% FA	73% CEM I-SR 7% FA 20% SF
Portlandite	$Ca(OH)_2$	10	−3.66	−3.73	−4.43
Ettringite	$Ca_6[Al(OH)_6]_2(SO4)_3.26H_2O$	10	2.46	2.31	0.92
Tobermorite	$Ca_5Si_6O_{17}.5H_2O$	10	9.77	9.11	8.36
Chabazite	$CaAl_2Si_4O_{12}.6H_2O$	10	3.41	3.18	5.03
Ettringite	$Ca_6[Al(OH)_6]_2(SO4)_3.26H_2O$	7	−7.25	−8.02	−8.12
Chabazite	$CaAl_2Si_4O_{12}.6H_2O$	7	10.71	9.62	9.98
CaP	$CaAl_2Si_{2.6}O_{9.2}.3.2H_2O$	7	7.51	6.74	6.95

Table 2
Chemical composition of leachates

Sample	pH	Alk (total)	Si(aq)	Ca	Na	K	Mg	SO_4^{2-}	Al	Fe
	mmol/l									
100% CEM I-SR	10.21	1.53	0.89	338	1.23	4.69	0.34	14.49	2.5×10^{-3}	1.2×10^{-3}
59% CEM I-SR+41% FA	10.18	1.30	0.73	333	2.04	8.54	0.33	14.43	3.7×10^{-3}	1.4×10^{-3}
73% CEM I-SR+7% FA+20% SF	9.83	0.98	1.06	328	2.41	6.93	0.47	14.73	2.1×10^{-3}	1.1×10^{-3}
100% CEM I-SR	7.16	0.04	2.85	348	0.98	1.02	5.32	15.69	1.5×10^{-2}	1.1×10^{-2}
59% CEM I-SR+41% FA	7.06	0.03	1.70	340	1.88	1.32	2.06	14.00	1.2×10^{-2}	1.1×10^{-2}
73% CEM I-SR+7% FA+20% SF	7.10	0.03	2.17	332	1.76	1.51	5.01	12.12	1.1×10^{-2}	1.3×10^{-2}

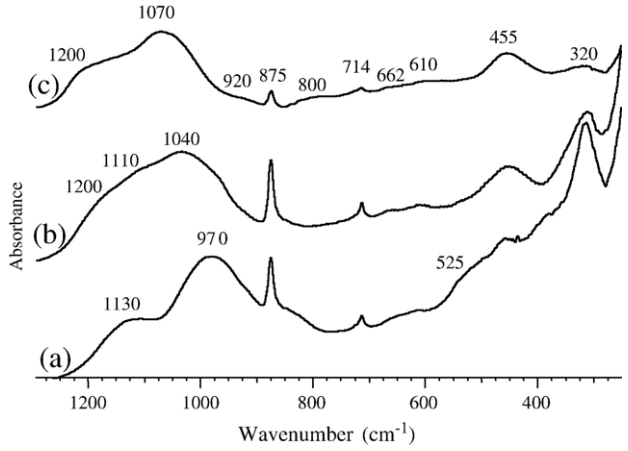

Fig. 1. Mid-IR spectra of a 100% CEM I-SR cement paste: (a) 100% CEM I-SR reference, (b) 100% CEM I-SR, pH=10, (c) 100% CEM I-SR, pH=7. Silicate environment. Undried KBr pellets.

The band located at ~610 cm^{-1}, which appears in leached samples, is also indicative of silicate and aluminosilicate glasses (symmetric stretching of Si–O–Si and Al–O–Si) [28].

The bands in the range 400–500 cm^{-1} are due to deformation of TO_4 tetrahedra (T=Si or Al), and the increasing in intensity of this bands, when leaching proceeds, is also consistent with an increasing in polymerization (more bridging TO_4 units linking dimers). Moreover, intensity of the out of plane bending Si–O vibration at 525 cm^{-1} decreases, when leaching proceeds, as a result of polymerization of SiO_4^{4-} units in cement.

Characteristic ettringite bands normally appear at 1100 and 610 cm^{-1} [32]. However, the Si–O stretching bands can eventually obscure the SO_4^{2-} bands of ettringite. In Fig. 1 broad bands centered at ~1110–1130 cm^{-1} can be attributed to C–S–H gels with Ca/Si<1.4 [27] overlapping ettringite main band.

According to Farmer [29], Al–O stretching vibrations of tetrahedral AlO_4 groups lie at 760–900 cm^{-1}. Band appearing at 800 cm^{-1} in sample leached at pH 7, which is assigned to stretching vibrations modes of O–T–O groups (T=Al, Si), is attributed to polymerization and Si replacement by Al in tetrahedral sites of C–S–H. However, in hydrated Portland cement pastes, Al is also found in octahedral coordination (ettringite, monosulfate and aluminate hydrate phase). Additionally Al has been detected by ^{27}Al MAS-NMR substituting Ca^{2+} ions in the interlayer structure of the C–S–H, and in a structurally unknown aluminate hydrate phase. The latter phase is tentatively assigned to a less crystalline alumina gel or calcium aluminate hydrate that includes $Al(OH)_6^{3-}$ or $O_xAl(OH)_{6-x}^{(3+x)-}$ octahedral in its structure [33,34]. The shoulder at 920 cm^{-1} may be assigned to OH bending vibrations in Al–OH–Al bonds (octahedral aluminium). The increase in intensity of these bands when leaching proceeds could be due to C_2AH_8, amorphous alumina gel, an unidentified calcium aluminate hydrate, the substitution of Ca by Al in the interlayer space of C–S–H or hydrogarnet precipitation [30,31,33,34].

The band at 320 cm^{-1} was due to Ca–O vibrations in portlandite and C–S–H gel. The decreasing in intensity was due to the dissolution of portlandite and decalcification of C–S–H gel.

The characteristic bands of calcite could be found at 1421, 874, and 713 cm^{-1}. Carbonation of samples is supposed to occur during the storing of samples previous to perform the microstructural characterization, and for this reason no interpretation of the bands and relation with the leaching process has been made.

The compensation of charge, needed after Si substitution by Al in tetrahedral sites, could be achieved incorporating additional H^+ from the acidic leaching media, in the interlayer space. The substitution of $(Al^{3+}+H^+)$ for Si^{4+} is an obvious possibility. However, the substitution of $2Al^{3+}$ for $(Si^{4+}+Ca^{2+})$ should also be considered [30,34].

Fig. 2 shows the OH stretching region for the mixture 100% CEM I-SR. Interpretation of the OH stretching region in the mid-IR spectra (~2800–3750 cm^{-1}) is difficult because bands are broad.

Evolution of the broad band at ~2800–3750 cm^{-1} is due to stretching vibrations of O–H groups in H_2O or hydroxyls with a wide range of hydrogen bond strengths. Band at 3640 cm^{-1} is due to Ca–OH vibrations from portlandite. The disappearing of this band when leaching proceeds allows us to follow the dissolution process of this solid phase. The band at 3450 cm^{-1} is attributed to hydrogen bonded OH species (O–H–O–H) adsorbed on the surfaces. The intensity of this band increases for leached samples with a C–S–H structure closed to tobermorite, i.e., with a lower Ca/Si ratio and polymerization of silicate chains, an increasing of the basal space and a high content of the less strongly hydrogen-bonded water molecules in the interlayer space. A shoulder, revealed at ~3600 cm^{-1} in pH=7 leached sample, was attributed to stretching OH vibrations in Al–OH bonds and it is another indication of the substitution of Ca for Al in the interlayer space of the C–S–H gel. [29].

Analyses of mid-IR spectra for cement pastes, including mineral additions (59% CEM I-SR+41% FA and 73% CEM I-SR+7% FA+20% SF), are presented in Figs. 3 and 4, respectively. FTIR data for these mixtures provide similar information. Small differences with the previously analysed data

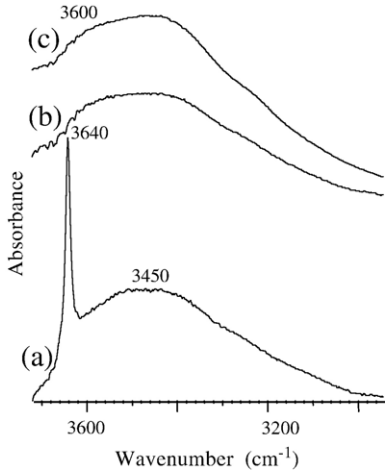

Fig. 2. Mid-IR spectra of a 100% CEM I-SR cement paste. OH environment: (a) 100% CEM I-SR reference, (b) 100% CEM I-SR, pH=10, (c) 100% CEM I-SR, pH=7. Dried KBr pellets.

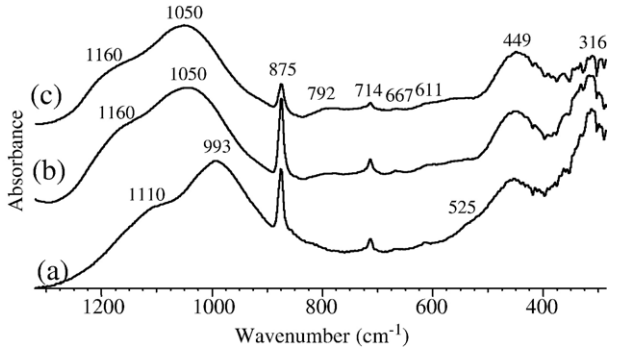

Fig. 3. Mid-IR spectra of a 59% CEM I-SR+41% FA cement paste: (a) 59% CEM I-SR+41% FA reference, (b) 59% CEM I-SR+41% FA, pH=10, (c) 59% CEM I-SR+41% FA, pH=7. Silicate environment. Undried KBr pellets.

could be attributed to differences in Ca/Si ratio in silicates for reference samples.

The shift of the Si–O stretching band, occurring at ~970 cm^{-1} for 100% CEM I-SR reference cement paste, to higher frequencies (compare Figs. 3 and 4 with Fig. 1) was due to the lower Ca/Si ratio in C–S–H gels for the mixtures of CEM I-SR+FA and CEM I-SR+FA and SF. The displacement of these bands with leaching progress occurred in all cases until ~1050 cm^{-1}, indicating decalcification up to a constant Ca/Si ratio was reached. The formation of shoulders at ~1160–1200 cm^{-1} indicated also the presence of C–A–S–H gels with Ca/Si<1.

Main fly ash band from Si–O and Al–O vibrations, located at 1080 cm^{-1} [28], could not be discerned due to interferences in absorption with the other mineral phases (see Fig. 3).

Main silica fume bands occur at 1120, 808 and 476 cm^{-1}. The disappearing of silica fume in leached samples for mixture 73% CEM I-SR+7% FA+20% SF could be followed through the decrease in the intensity of the band at 1120 cm^{-1} in Fig. 4. The bands in the range 400–500 cm^{-1}, due to deformation of TO_4 tetrahedra (T=Si or Al), are in this case superposed with band of silica fume, and, for this reason, they change in intensity and slightly in frequency.

Al–O stretching bands at 800 cm^{-1}, attributed to the silicon substitution for aluminium in C–S–H, appear in blended cement pastes in samples leached until an equilibrium pH of 10 (T–O

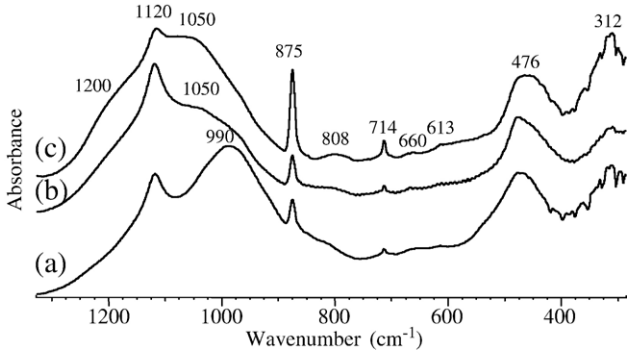

Fig. 4. Mid-IR spectra of a 73% CEM I-SR+7% FA+20% SF cement paste: (a) 73% CEM I-SR+7% FA+20% SF reference, (b) 73% CEM I-SR+7% FA+20% SF, pH=10, (c) 73% CEM I-SR+7% FA+20% SF, pH=7. Silicate environment. Undried KBr pellets.

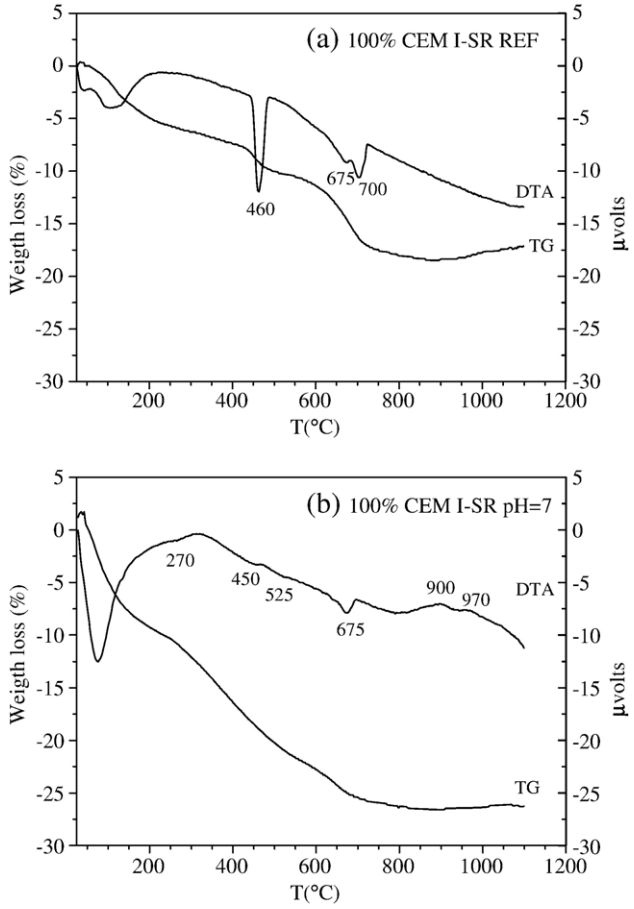

Fig. 5. DTA and TG curves for 100% CEM I-SR cement pastes. Fig. 5-a, reference cement paste. Fig. 5-b, cement paste leached until pH=7.

stretching vibrations, ~1050 cm^{-1}). This fact is an indication that aluminium could substitute silicon when a C–S–H gel with a low Ca/Si ratio was formed. The formation of a C–A–S–H matrix could be due to the decalcification process associated with leaching and/or to the pozzolanic reaction with mineral admixtures. Looking at FTIR curves of reference materials in Figs. 3 and 4, we can conclude that the addition of mineral admixtures, such as silica fume and fly ash, to cement pastes causes the formation of a more polymerized and low Ca form of C–S–H gel, obtained by the reaction between the pozzolan with portlandite and the typical high-Ca form of C–S–H gel [19].

The term geopolymer was first used by Davidovits [35] to describe a family of mineral binders closely related to artificial zeolites. These structures consist of a polymeric Si–O–Al framework, similar to that found in zeolites, being the main difference with zeolitic structures that geopolymers are X-ray amorphous. The leaching of a Portland or blended Portland cement paste is characterized by a number of stages that are reflected in silicate and water regions by FTIR data. Formation of a C–A–S–H matrix, with a structure with Al in IV fold coordination, and probable additional presence of a mineral phase with Al in VI fold coordination, is concluded from mid-IR spectra. However, amorphous C–A–S–H matrices have broad, unresolved bands, and could be difficult to distinguish them in a mixture of minerals.

3.3. Thermal analysis

Fig. 5 presents the thermogravimetric (TG) and differential thermal analysis (DTA) curves for the reference hydrated Portland cement paste (CEM I-SR) (Fig. 5-a) and the same paste leached until equilibrium was reached at pH=7 (Fig. 5-b). For reference sample (Fig. 5-a), the weight loss peak around 100 °C is induced by hygroscopic water (i.e. physically absorbed water). Zone between 100 and approximately 200 °C is attributed to dehydration of C–S–H gel. The step at 425–550 °C is due primarily to decomposition of portlandite. Carbonates show distinctive decomposition peaks at the temperature range of 625–875 °C. The loss below the portlandite step is due to decomposition of C–S–H and the hydrated aluminate phases, but in this zone cement pastes show only slight indications of steps. The absence of steps is probably due to a combination of low crystallinity, the presence of other phases and the presence of AFm phases of different compositions in mixture or solid solution or both.

Leached sample (Fig. 5-b) shows from 200–300 °C a valley due to dehydration of hydrated aluminosilicates of undefined composition. Endothermic valleys ranging 450–550 °C in DTA curve of leached sample are related also with different steps of the dehydration process in silicoaluminates with structure similar to zeolites [36,37].

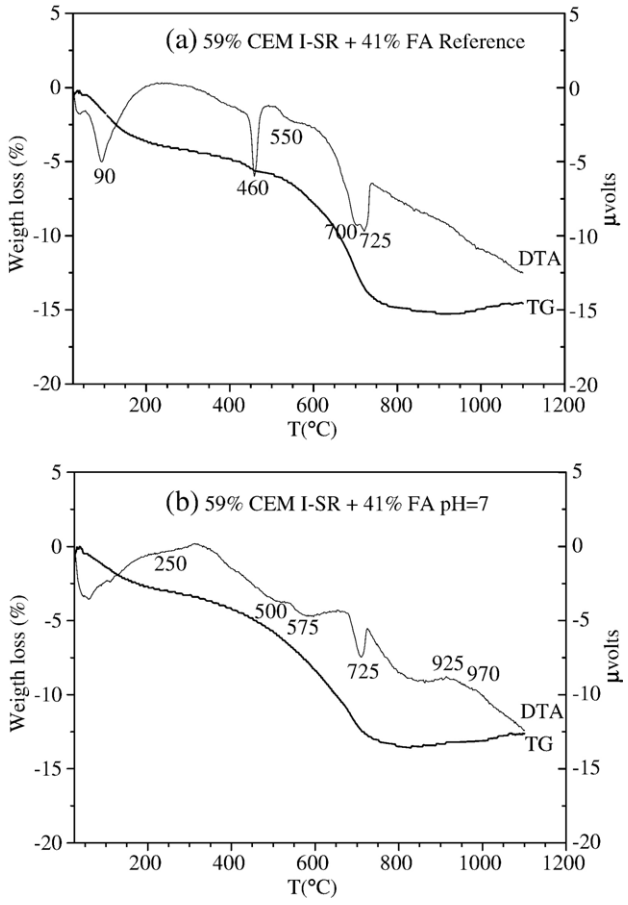

Fig. 6. DTA and TG curves for 59% CEM I-SR+41% FA cement pastes. Fig. 6-a, reference cement paste. Fig. 6-b, cement paste leached until pH=7.

Table 4
BET surface area (S_T), BJH-adsorption pore volume (V_P) and BJH-adsorption mean pore diameter (D_m) for the studied samples

Sample	Cement mixture	Remarks	S_T [m^2g^{-1}]	V_P [cm^3g^{-1}]	D_m [Å]
1	100% CEM I-SR	Reference	5	0.03	181
2	100% CEM I-SR	Leached pH=10	42	0.16	147
3	100% CEM I-SR	Leached pH=7	88	0.27	107
4	59% CEM I-SR+41% FA	Reference	7	0.03	155
5	59% CEM I-SR+41% FA	Leached pH=10	28	0.08	120
6	59% CEM I-SR+41% FA	Leached pH=7	38	0.12	134
7	73% CEM I-SR+7% FA+20% SF	Reference	8	0.03	142
8	73% CEM I-SR+7% FA+20% SF	Leached pH=10	33	0.11	138
9	73% CEM I-SR+7% FA+20% SF	Leached pH=7	31	0.11	133

The exothermic peaks at 900 and 970 °C are assigned to the breakdown to wollastonite of silicoaluminates type Al-susbstituted tobermorite, with different amounts of Al substituting Si. Mitsuda et al. [38,39] found a broad exothermic peak at 830 °C for pure not substituted tobermorite, and strong exothermic peaks for substituted tobermorite at high temperatures. Samples with increasing Al content would exhibit the exothermic effect at progressively increasing temperatures [30,37]. The flatted form of the exothermic peaks is related, according to Kalousek [30], to a high fineness due to the relatively high Al content.

Fig. 6 presents the TG and DTA curves for the reference hydrated fly ash-Portland cement paste (59% CEM I-SR+41% FA) (Fig. 6-a) and the same paste leached until pH=7 (Fig. 6-b). Reference sample show the endothermic peaks of portlandite (460 °C) and calcite (700–725 °C), and a valley at 550 °C that can be attributed either to dehydration of mullite from fly ash or to the presence of silicoaluminates in reference sample produced in the pozzolanic reaction.

The identification of mineral components and their quantification, using DTA/TGA is difficult and often may be impossible due to overlapping processes. However the presence of endothermic valleys for leached samples, at temperature ranges of 200–300 °C and 470–550 °C, reveal the presence of Si–OH and Al–OH groups, produced during the breakdown of Si–Si or Al–Si bonds in polymerised silicoaluminate chains.

3.4. Nitrogen adsorption

For the reference materials (samples 1, 4 and 7) the measured values for BET surface area (S_T) and pore volume (V_P) were about 5 $m^2\ g^{-1}$ and 0.03 $cm^3\ g^{-1}$, respectively. Both values invariably increased after processing (Table 4). For the series 1 to 3 (100% CEM I-SR) the increase on S_T and V_P when leaching proceeds, was in consonance with a decrease of the medium pore diameter (D_m) values. Fig. 7-a shows that in sample 1 (100% CEM I-SR reference), approx. 65% of the pores had a diameter larger than 350 Å. For samples 2 (100% CEM I-SR

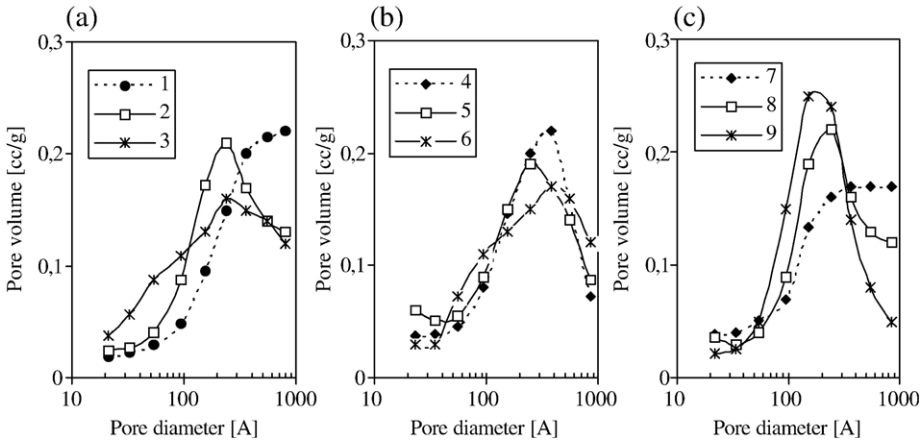

Fig. 7. BJH-adsorption pore volume plots (dV/dlogD) for series (a) 1 (100% CEM I-SR reference), 2 (100% CEM I-SR pH 10) and 3 (100% CEM I-SR pH 7); (b) 4 (59% CEM I-SR 41% FA reference), 5 (59% CEM I-SR 41% FA pH 10) and 6 (59% CEM I-SR 41% FA pH 7), and (c) 7 (73% CEM I-SR 7% FA 20% SF reference), 8 (73% CEM I-SR 7% FA 20% SF pH 10) and 9 (73% CEM I-SR 7% FA 20% SF pH 7).

leached until pH=10), and 3 (100% CEM I-SR leached until pH=7) this value was reduced to 40% in both cases. For sample 2 the major part (approx. 40%) of the pore volume had a pore diameter in the range of 150–250 Å; only 20% of the pores had a diameter smaller than 150 Å. Sample 3 had the largest proportion (approx. 30%) of pore volume assigned to pores smaller than 100 Å in diameter. For CEM I-SR+FA (series 4 to 6) a similar behavior was observed. However, estimated value of D_m for sample 6 (59% CEM I-SR+41% FA leached until pH=7), was slightly larger than that of sample 5 (59% CEM I-SR+41% FA leached until pH=10), likely due to the closure of mesopores that were already present on sample 5 (see Fig. 7-b area between 20 and 50 Å pore diameter). For CEM I-SR+FA+SF (series 7 to 9), the increase in S_T and V_P together with a decrease on mean pore diameter was only observed when comparing either samples 7 (73% CEM I-SR+7% FA+20% SF reference), and 8 (73% CEM I-SR+7% FA+20% SF leached until pH=10) or 7 (73% CEM I-SR+7% FA+20% SF reference), and 9 (73% CEM I-SR+7% FA+20% SF leached until pH=7). The leached samples 8 and 9 showed a very much alike behavior with respect to the mentioned parameters. Main differences were found only after analyzing the plot of pore size distribution (Fig. 7-c). The estimated proportion of pore volume for large pore sizes (in the range of 350 to 850 Å) was of 0.51%, 0.41% and 0.27% for samples 7, 8 and 9, respectively. Hence, sample 9 showed a significant reduction in the amount of pores with large diameter when compared to sample 8.

In general, an increase in surface area with leaching is found. The leaching process allows passing from a high-density C–S–H structure, to a lower density C–A–S–H structure with a higher surface area and a higher internal porosity composed mainly of gel pores (1–100 nm). This fact is in agreement with the link between low density silicate or silicoaluminate gels, and the layered mineral tobermorite.

4. Conclusions

This work shows that the leaching of pastes based in Portland cements produces a geopolymeric structure closely related to artificial zeolites. These C–A–S–H structures consist of a polymeric Si–O–Al framework, similar to that found in zeolites, and they can be considered zeolite precursors. From a thermodynamic point of view the leaching of Portland cement based materials, due to the decreasing of pH, is a complex process governed by the combination of dissolution and precipitation processes, such as:

- Dissolution of portlandite.
- Decalcification of C–S–H gel.
- Silicate polymerisation.
- Incorporation of tetrahedral and/or hexagonal aluminium in polymerised gel resulting in the formation of an aluminosilicate gel.

The new formed C–A–S–H matrix has a higher surface area, an increase in internal porosity (gel pores), and a higher interlayer water content typical of low density “gels”.

Cements conditioned to form aluminosilicates with a structure similar to zeolites, can act also as adsorbents for waste species. Zeolitic materials are known for their abilities to adsorb toxic chemical wastes.

Acknowledgement

The financial support of Région Poitou-Charentes (Convention 04/RPC-R-120) is greatly acknowledged.

References

[1] H.F.W. Taylor, Cement Chemistry, Academic Press, New York, 1990.
[2] Z. Xu, D. Viehland, Observation of a mesostructure in calcium silicate hydrate gels of portland cement, Phys. Rev. Lett. 77 (1996) 952–955.
[3] E.P. Flint, L.S. Wells, Study of the system CaO–SiO_2–H_2O at 30 °C and the reaction of water on the anhydrous calcium silicates, J. Res. Natl. Bur. Stand. 12 (1934) 751–783.
[4] P.S. Roller, J.G. Ewin, The system calcium oxide–silica–water at 30·C. The association of silicate in dilute alkaline solution, J. Am. Chem. Soc. 62 (1940) 461.
[5] H.F.W. Taylor, Hydrated calcium silicates. Part I, compound formation at ordinary temperatures, J. Chem. Soc. 275 (1950) 3682–3690.

[6] S.A. Greenberg, T.N. Chang, E. Anderson, Investigation of Colloidal Hydrated Calcium Silicates I. Solubility products, J. Phys. Chem. 64 (1965) 1151–1157.
[7] S.A. Greenberg, T.N. Chang, Investigation of Colloidal Hydrated Calcium Silicates II. Solubility relationships in the calcium oxide–silica–water system at 25 °C, J. Phys. Chem. 69 (1965) 182–188.
[8] K. Fujii, W. Kondo, Heterogeneous equilibrium of calcium silicate hydrate in water at 30 °C, J. Chem. Soc. Dalton Trans. 2 (1981) 645–651.
[9] F.P. Glasser, E.E. Lachowski, D.E. Macphee, Compositional model for calcium silicate hydrate (C–S–H) gels, their solubilities, and free energies of formation, J. Am. Ceram. Soc. 70 (1987) 481–485.
[10] S.A. Hamid, The crystal structure of 11A natural tobermorite $Ca_{2.25}[Si_3O_{7.5}(OH)_{1.5}].1H_2O$, Z. Kristallogr. 154 (1981) 189–198.
[11] S. Merlino, E. Bonaccorsi, T. Armbruster, Tobermorites: their real structure and order–disorder (OD) character, Am. Mineral. 84 (1999) 1613–1621.
[12] X. Cong, R.J. Kirkpatrick, 29Si MAS NMR study of the structure of calcium silicate hydrate, Adv. Cem. Based Mater. 3 (1996) 144–156.
[13] I. Klur, Etude par RMN de la structure des silicates de calcium hydratés, Thesis Université Paris 06, Paris (1996).
[14] I. Klur, B. Pollet, J. Virlet, A. Nonat, CSH structure evolution with calcium content by multinuclear NMR, in: P. Colombet, A.-R. Grimmer, H. Zanni, P. Sozzani (Eds.), Nuclear Magnetic Resonance Spectroscopy of Cement-Based Materials, Springer, Berlin, 1998, pp. 119–141.
[15] S. Shaw, S.M. Clark, C.M.B. Henderson, Hydrothermal formation of the calcoium silicate hydrates, tobermorite ($Ca_5Si_6O_{16}(OH)_2.4H_2O$) and xonotlite ($Ca_6Si_6O_{17}(OH)_2$): an in situ synchrotron study, Chem. Geol. 167 (2000) 129–140.
[16] S.A. Rodger, G.W. Groves, N.J. Clayden, C.M. Dobson, Hydration of tricalcium silicate followed by silicon-29 NMR with cross-polarization, J. Am. Ceram. Soc. 71 (1988) 91–96.
[17] M. Grutzeck, A. Benesi, B. Fanning, Silicon-29 magic angle spinning nuclear magnetic resonance study of calcium silicate hydrates, J. Am. Ceram. Soc. 72 (1989) 665–668.
[18] P. Faucon, J.M. Delaye, J. Virlet, Molecular dynamics simulation of the structure of calcium silicate hydrates. I. $Ca_{4+x}Si_6O_{14+2x}(OH)_{4-2x}(H_2O)_2$ ($0<x<1$), J. Solid State Chem. 127 (1996) 92–97.
[19] J.J. Thomas, J.J. Chen, A.J. Allen, H.M. Jennings, Effects of decalcification on the microstructure and surface area of cement and tricalcium silicate pastes, Cem. Concr. Res. 34 (12) (2004) 2297–2307.
[20] A.W. Harris, M.C. Manning, W.M. Tearle, C.J. Tweed, Testing of models of the dissolution of cements-leaching of synthetic C–S–H gels, Cem. Concr. Res. 32 (2002) 731–746.
[21] T. Fujita, D. Sugiyama, S.W. Swanton, B.J. Myatt, Observation and characterisation of colloids derived from leached cement hydrates, J. Contam. Hydrol. 61 (2003) 3–16.
[22] A. Hidalgo, C. Andrade, C. Alonso, Evaluation of the long term behaviour of concrete used in high level nuclear waste disposal (HLW). An accelerated leaching test, in: G. Ortiz de Urbina, H. Goumans (Eds.), Environmental and Technical Implications of Construction with Alternative Materials, Iscowa-Inasmet, San Sebastian, 2003, pp. 857–860.
[23] A. Hidalgo, C. Andrade, C. Alonso, An accelerated leaching test to evaluate the long term behaviour of concrete in waste disposal, Ind. Ital. Cem. 766 (2001) 498–507.
[24] L.N. Plummer, D.L. Parkhurst, G.W. Fleming, S.A. Dunkle, A computer program incorporating Pitzer's equations for calculation of geochemical reactions in brines, U.S. Geological Survey, Water Resources Investigations Report, vol. 88-4153, U.S. Geological Survey, Reston, 1988.
[25] J.E. Cross, F.T. Ewart, HATCHES a thermodynamic database and management system, Radiochim. Acta 52/53 (1991) 421–422.
[26] R.Sh. Mikhail, L.E. Copeland, S. Brunauer, Pore structures and surface areas of hardened Portland cement pastes by nitrogen adsorption, Can. J. Chem. 42 (1964) 426–438.
[27] P. Xu, R.J. Kirckpatrick, B. Poe, P.F. McMillan, X. Cong, Structure of calcium silicate hydrate (C–S–H): near-, mid-, and far-infrared spectroscopy, J. Am. Ceram. Soc. 82 (3) (1999) 742–748.
[28] W.K.W. Lee, J.S.J. van Deventer, Structural reorganisation of class F fly ash in alkaline silicate solutions, Colloids Surf., A Physicochem. Eng. Asp. 211 (2002) 49–66.
[29] V.C. Farmer, The Infrared Spectra of Minerals, Mineralogical Society, London, 1974.
[30] G.L. Kalousek, Crystal chemistry of hydrous calcium silicates: I. Substitution of aluminium in lattice of tobermorite, J. Am. Ceram. Soc. 40 (3) (1957) 74–80.
[31] S. Diamond, J.L. White, W.L. Dolch, Effects of isomorphous substitution in hydrothermally-synthesized tobermorite, Am. Mineral. 51 (1966) 388–402.
[32] F. Farcas, Ph. Touzé, La spectrométrie infrarouge à transformée de Fourier (IRTF). Une méthode intéressante pour la caractérisation des ciments, Bull. Lab. Ponts Chaussées 230 (2001) 77–88.
[33] M.D. Andersen, H.J. Jakobsen, J. Skibsted, Incorporation of Aluminium in the C–S–H of hydrated Portland cements: a high-field ^{27}Al and ^{29}Si MAS-NMR investigation, Inorg. Chem. 42 (7) (2003) 2280–2287.
[34] P. Faucon, A. Delagrave, J.C. Petit, C. Richet, J.-M. Marchand, H. Zanni, Aluminium incorporation in calcium silicate hydrates (C–S–H) depending on their C/S ratio, J. Phys. Chem., B 103 (37) (1999) 7796–7802.
[35] J. Davidovits, Ancient and modern concretes: what's the real difference? Concr. Int. (December 1987) 23–35.
[36] A. Langella, M. Parsini, G. larri, P. Cappelletli, M. de Gennaro, Thermal behaviour of natural and cation-exchanged clinoptilolite from Sardinia (Italy), Clays Clay Miner. 51 (6) (2003) 625–633.
[37] S. Shaw, C.M.B. Henderson, B.U. Komanschek, Dehydration/recrystallization mechanisms, energetics, and kinetics of hydrated calcium silicate minerals: an in situ TGA/DSC and synchrotron radiation SAXS/WAXS study, Chem. Geol. 167 (2000) 141–159.
[38] T. Mitsuda, Synthesis of tobermorite from zeolite, Mineral. J. 6 (3) (1970) 143–158.
[39] T. Mitsuda, H.F.W. Taylor, Normal and anomalous tobermorites, Mineral. Mag. 42 (1978) 229–235.